https://doi.org/10.2352/ISSN.2470-1173.2017.11.IMSE-078

Accurate Joint Geometric Camera Calibration of Visible and Far-Infrared Cameras

Takashi Shibata*[1,2]*, Masayuki Tanaka*[1]*, and Masatoshi Okutomi*[1]*;* [1] *Tokyo Institute of Technology, Tokyo, Japan,* [2] *NEC corporation, Kanagawa, Japan

Abstract

This paper presents a novel joint geometric camera calibration system using a novel calibration target for a visible and a far-infrared (FIR) cameras. By using the proposed calibration target which is the two-layer structure with different combinations of thermal emission, we can stably and precisely obtain the corresponding points of the checker pattern in the calibration target from the visible and the FIR images. The simple calibration algorithm based on the well-known Zhang's algorithm can accurately estimate the camera parameters, because we can use many useful tools which contribute the accuracy. Experimental results show that the proposed calibration system enables us to easily calibrate the visible and the FIR image with high accuracy compared with an existing system. Furthermore, the proposed system can lead to develop various applications including joint image denoising, and joint image up-sampling.

Introduction

Multi-spectral and multi-modal images are becoming common in image processing [1, 2, 3, 4, 5, 6, 7, 8, 9, 10], computational photography [11, 12, 13, 14] and computer vision [15, 16, 17, 18]. Particularly, far-infrared (FIR) imaging is effective for night vision [19, 20], pedestrian detection [21, 22, 23], and temperature analysis [24, 25], because the FIR is robust to low-light condition and lightning changes [26]. To obtain these benefits of the FIR image properties, image processing algorithms which is focusing on a joint use of visible and FIR image pairs have been proposed. For example, various image fusion methods for the visible and FIR image pairs have been proposed [27, 28, 29, 30, 31, 32, 33]. Surface temperature analysis techniques [34, 35] and pedestrian detection algorithm [36] using the visible and the FIR image pairs were presented. For these methods, an accurate joint calibration between the visible and the FIR camera pairs is required.

For joint calibration for visible camera pairs, various effective methods have been proposed. Among them, the most standard approach is to use a planner calibration board with a printed checker pattern. The very effective algorithm using the checker pattern was proposed by Zhang [37]. In the Zhang's algorithm, the corresponding points, e.g. grid corners, located on each planes are extracted using a corner extraction algorithm. The intrinsic and the extrinsic camera parameters are estimated by minimizing the reprojection error between the world coordinate and the each image coordinate. Furthermore, many open sources based on highly sophisticated implementations such as the Caltech MATLAB Calibration tool box [38] and Open CV [39] are available. These implementations also include many useful tools which contribute the calibration accuracy.

Contrary to the accumulated progress of the joint calibration techniques for the visible camera pairs, the joint calibration for the visible and the FIR camera pairs is still challenging. For the FIR camera calibration, bright spots such as small light bulbs or a modified laser pointer are often used as the calibration points [40]. The specially designed targets for the FIR camera using a wire grid object [24] or a special planer board [41, 42, 43, 44, 45, 46] were also presented. However, these calibration methods are not applicable to the joint calibration for the visible and the FIR cameras, because it is very difficult to extract corresponding points between both images.

To conduct the joint calibration of the visible and the FIR cameras, a specially designed target based on a geometric mask with high thermal contrast was presented [47]. Although the mask-based approach can capture the corresponding points between the visible and the FIR images, the calibration accuracy is still insufficient. The alternative approach for the joint calibration is to employ the Zhang's algorithm [37] using the checker pattern [34, 18, 48]. In these methods, the calibration target is heated by a flood lump or hot air to visualize the checker pattern in the FIR image. Although the Zhang's algorithm can be utilized, the performance of the calibration for the FIR camera is still limited. This is because the extracted corresponding point coordinate, which is critical for the Zhang's algorithm, is inaccurate and unstable due to the unclear checker pattern in FIR image.

This paper presents a novel joint camera calibration system for the visible and the FIR cameras. The main contribution of this paper is to present the simple but accurate calibration for visible and FIR cameras by using the proposed calibration target which is capable of obtaining stably and precisely the clear corresponding points of the checker pattern from the visible and the FIR images. Experimental results show that the proposed calibration flow enables us to easily calibrate the visible and the FIR image with high accuracy compared with a existing method. Furthermore, the proposed system can lead to develop various applications including joint image denoising, and joint image up-sampling.

Proposed method

The overview of the proposed calibration flow is shown in Fig. 1. The proposed flow consists of the five steps: 1) calibration for a visible camera, 2) tone mapping for a FIR image, 3) calibration for the FIR camera, 4) extrinsic parameter estimation, and 5) image alignment. In the proposed system, we first capture the visible and the FIR images simultaneously which include the corresponding checker pattern by the proposed calibration target as

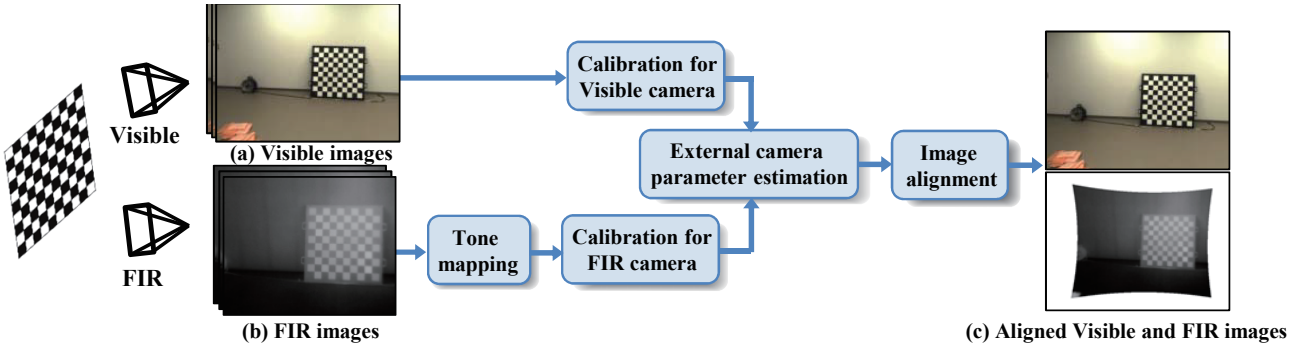

Figure 1. *Overall flow of our proposed joint calibration flow.*

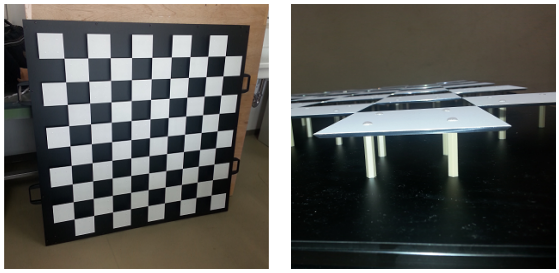

(a) Front view (b) Side view

Figure 2. *Proposed calibration target.*

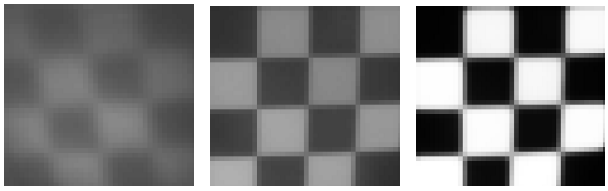

(a) Existing system (b) Proposed system (before tone mapping) (c) Proposed system (after tone mapping)

Figure 3. *Captured FIR images.*

shown in Fig. 1 (a) and (b). Then, the tone mapping is applied to the captured FIR image to enhance the captured checker pattern. The intrinsic parameters of the visible and the FIR cameras are estimated. Next, the extrinsic camera parameters between both cameras are estimated. Finally, the both images are aligned using the estimated intrinsic and extrinsic camera parameter as shown in Fig. 1 (c).

Proposed calibration target

The proposed calibration target is shown in Fig. 2 (a). The proposed target consists of the two layers: 1) the black and planner base board and 2) the white planner plates. Here, the white plates which are held up by poles as shown in Fig. 2 (b). The black base board is made of resin whose thermal infrared emissivity is very small, while the white planner plates is made of aluminum. The surfaces of the plates are painted by resin whose thermal emissivity is large. The FIR images which contain the proposed calibration target is shown in Fig. 1 (b). The region in the base board is dark due to the small emissivity of the base board, while the region in the planner plates are bright (i.e. high temperature) originated from the thermal radiation from the resin on the plates.

In the existing calibration target by Prakash's system [34], the checker pattern in the FIR image is blurred due to the thermal diffusion between the high temperature and the low temperature regions as shown in Fig. 3 (a). Contrary to the existing calibration target, the proposed calibration target can produces the sharp checker pattern as show in Fig. 3 (b). The reason for this is that the bright and the dark regions are thermally insulated by the two-layer structure of the proposed calibration target, because the boundary between base board and the white plates are unconnected.

Furthermore, the low thermal diffusion structure is also very effective to persist the clear checker pattern for a long time (>15 min.). Note that this persistence is critical to stably capture the checker pattern in the FIR camera. The persistence also leads to dramatically reduce the required time for obtaining the set of images for calibration. As shown in Fig. 1 (a) and (b), we can obtain the corresponding checker pattern from the visible and the FIR images simultaneously, which is necessary for the joint calibration for the visible and the FIR cameras.

Tone mapping for FIR image

In the proposed system, a clear checker pattern can be obtained by using our calibration target as shown in Fig. 3 (b). In general, however, compared with the checker pattern of the visible image, the intensity difference between the bright region and the dark region in the FIR image is much smaller than that of the visible image. To apply the corner detection algorithm which is designed for the visible image directly, we enhance the bright and the dark regions in the FIR image by using our tone mapping algorithm. Our tone mapping is designed so that the intensity in the bright and the dark region is adaptively mapped into the white and the black for each pixel. More specifically, our tone mapping function f is given by

$$I_j = f(I_j) = 128 \times \left[\tanh\left(\eta \frac{(I_j - I_j^{med})}{(I_j^{up} - I_j^{low})}\right) + 1\right], \quad (1)$$

where I_j is the input FIR image intensity of j-th pixel, I_j^{up}, I_j^{low} are the mean intensity of the nearest bright square and the nearest dark square for j-th pixel, I_j^{med} is given by $I_j^{med} = (I_j^{up} + I_j^{low})/2$, and η is the parameter which determines the slope width of the hyperbolic function in f. In the following of this paper, we set

η as 0.5. As shown in Fig. 3 (c), we can generate the clearer checker pattern by applying our tone mapping algorithm, because the original intensity of the FIR image is adaptively mapped into the white and the black for each pixel based on the intensity of the nearest bright and the dark square.

Camera calibration and image alignment

In the proposed system, the basic pinhole camera model is employed for our calibration system. Let $\mathbf{x} = (x_n, y_n, 1)^T$ and $\mathbf{X} = (X, Y, Z, 1)^T$ be the image coordinate and the world coordinate, respectively. The transformation from the world coordinate to the image coordinate is given by $\lambda\mathbf{x} = \mathbf{K}[\mathbf{R}|\mathbf{t}]\mathbf{X}$, where λ is an arbitrary scale parameter, $\mathbf{K}$ is the camera intrinsic matrix, $\mathbf{R}$ is the rotation matrix, and $\mathbf{t}$ is the translation vector, receptively. In general, the captured image is distorted due to the optical lense. In this paper, the widely used distortion model [38] which approximates the radial and tangential distortion is employed.

In the proposed system, we can obtain the accurate extrinsic camera parameter between the visible and the FIR cameras by using this camera calibration model and the proposed calibration target. The reason for this is that we can extract the corresponding corner from the corresponding checker pattern from the visible and the FIR images simultaneously by using the proposed calibration target.

Finally, the FIR image is aligned into the visible image coordinate using the estimated camera parameter. The depth information is required for the image alignment. In our setting, we can assume that the baseline between the visible and the FIR cameras is much smaller than the depth of each object. Therefore, we can set a fixed depth to align the two images, because the disparity originated from the subject distance deferences is negligible.

In the proposed method, the Caltech MATLAB Calibration tool box [38] is used to estimate the intrinsic parameters of the visible and the FIR cameras and the extrinsic parameters between both cameras. By employing the Zhang's algorithm with the highly sophisticated implementation including many useful tools, we can estimate the camera parameters with high accuracy.

Experiments

To evaluate the performance of the proposed calibration system, we set a joint image capturing device composed of a visible and a FIR camera. We used POINT GREY Firefly MV for the visible camera and FLIR A15 for the FIR camera, whose resolutions are 640x480 and 160x128 pixel, respectively. In the following of this section, we first evaluate the effectiveness of the proposed calibration target and the accuracy of the proposed calibration system. Next, the applications using the proposed system are demonstrated.

Calibration accuracy evaluation

We can simultaneously obtain the clear checker pattern for a long time by the proposed calibration target with our tone mapping algorithm. This strength is critical to stably extract the corresponding points from the FIR images. This is because we can estimate the accurate camera parameters using the Zhang's algorithm [37] which is supported by the sophisticated implementations and the useful tools, if the accurate corresponding points are extracted.

To show the stability of the extracted corresponding points

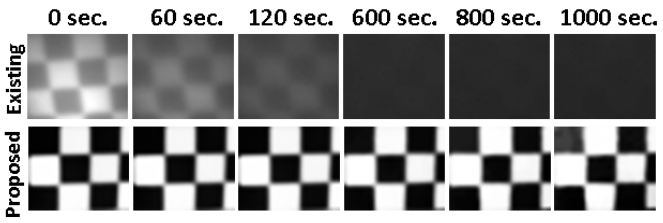

Figure 4. *Progress of checker pattern in FIR image by existing [34] and proposed system.*

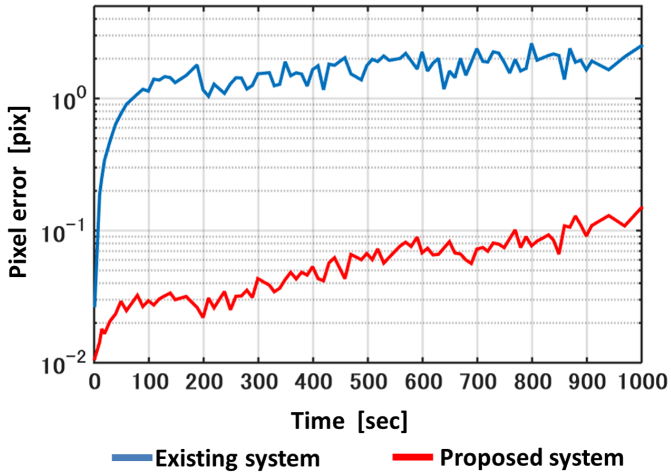

Figure 5. *Stability of extracted corresponding points by existing [34] and proposed system.*

by the proposed calibration target, we captured the set of the checker patterns in the FIR images over 1,000 [sec] and evaluated the time series variation of the extracted points from the FIR images. To compare the performance of the proposed target with a existing target, the same experiments were conducted by Prakash's approach [34]. In the experiment, the calibration target which includes 25 grids were used. Note that the calibration target for the existing method [34] was also designed so that the size of the checker pattern was same as that of the proposed one.

An example of the captured checker pattern for the existing and the proposed system are shown in Fig. 4. Here, the top and the bottom row show the checker pattern by the existing and the proposed system. Each column shows the time series variation of the checker pattern just after heating. As shown in Fig. 4, the checker pattern by the proposed target is much clearer than that of the existing target over all times. Furthermore, the clear checker pattern by the proposed target can be preserved after 600 [sec], while the checker pattern by the existing target is quickly diminished.

To evaluate quantitatively the stability of the extracted corresponding points, we measured the mean square error between the extracted point coordinates at initial time and that of each time. The time series variation of the error is shown in Fig. 5. Here, the smaller pixel error is, the more stable the extracted corresponding points is. As shown in Fig. 5, the errors by the proposed target is smaller than 0.1 pixel even after 800 [sec], while the error by

Table 1. Mean reprojection error for visible and FIR images

Calibration system	FIR image	Visible image
Existing (Prakash's [34])	0.1841 [pix]	2.360 [pix]
Proposed	0.0676 [pix]	0.139 [pix]

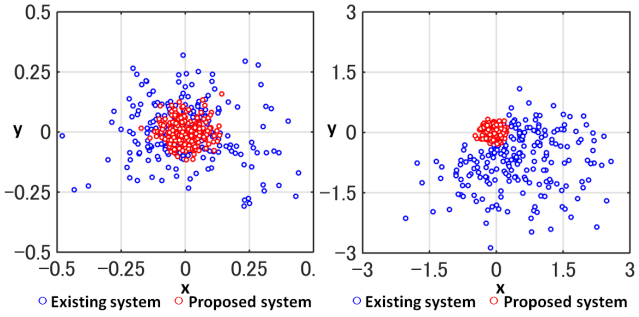

(a) FIR image (b) Visible image

Figure 6. *Scatter plot of reprojection error of existing [34] and proposed system.*

(a) input FIR image

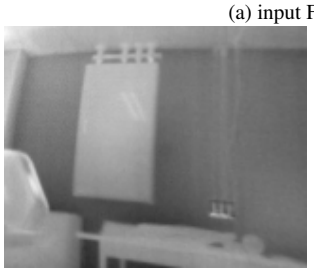

(b) Result by existing system [34]

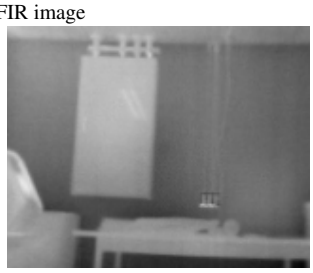

(c) Result by proposed system

Figure 7. *Input and distortion corrected FIR images.*

the existing approach is larger than one pixel after 60 [sec]. The results show the stability of the extracted corresponding points by the proposed target compared with the existing one.

Next, the accuracy of the intrinsic and the extrinsic camera parameters by the proposed and the existing system was examined. We captured the 60 images. Among them, we used 30 images to calibrate both cameras. The other 30 images were used for evaluation. To evaluate the performance, we measured the mean reprojection error (MRE), i.e. the residual between the extracted point coordinate of each image and the transformed point coordinate from the world coordinate into each image coordinate using the estimated camera parameters by the proposed and the existing system.

The evaluation results of each MRE are shown in Table. 1. The scattering plots corresponding to each MRE are also shown in Fig. 6 (a) and (b). Here, the red and blue points show the residual by the proposed and the existing system, respectively. As shown Fig. 6, the error by the proposed system is much smaller than that of the existing method [34]. Note that the error in the visible image by the exiting system is much worse than that of the proposed system as shown in Fig. 6 (b), even though the accuracy of the estimated intrinsic parameter of the visible image is same. In our calibration, the extrinsic parameters of the visible and the FIR cameras are jointly estimated using the estimated intrinsic parameters of both cameras. Therefore, the inaccurate intrinsic parameter of the FIR camera directly affects the accuracy of the estimated extrinsic parameters of both cameras. An example of the effectiveness of the accurate proposed joint calibration is shown in Fig. 7. The proposed system successfully generate the distorted FIR image as shown in Fig. 7 (c), while as shown in Fig. 7 (b), the distorted image by the existing system cannot remove the distortion completely. These results show that the proposed system can estimate both the intrinsic camera parameter of the FIR camera and the extrinsic parameter between the visible and the FIR cameras with high accuracy.

Applications of our joint calibration system

The accurate joint calibration result by the proposed system is effective for various applications such as joint image denoising, joint image up-sampling, and image fusion. In the following of this section, we demonstrate the example of these applications.

Image denoising

The first example is the joint image denoising application. Here, the denoising is carried out by guided filter [50]. The noisy visible image, the FIR image and the denoised results with the common visible image denoising method [49] and the proposed approach are shown in Fig. 8, respectively. The noisy visible image is generated by adding the Gaussian white noise ($\sigma = 35$) to the original image shown in Fig. 8 (f).

The close-ups of the red square are also shown in the left below of each image. As shown in Fig. 8 (a) and (b), the structure of the cable is unclear due to the large noise in the visible image, while the structure is clear in the FIR one. The existing method [49] cannot remove the noise sufficiently as shown in Fig. 8 (c). As shown in Fig. 8 (d), the structure of the black wire becomes unclear by existing system [34], because the misalignment exists between the visible and the FIR image. On the other hand, Fig. 8 (e) shows that the proposed approach can recover the structure by removing the noise, because the noise is effectively removed using the FIR image as the guide.

Image up-sampling

Finally, we demonstrate the effectiveness for the joint image up-sampling application. The up-sampling image is generated by refining the aligned FIR image using the guided filter [50]. The visible image, the FIR image and the up-sampled results with the proposed calibration system are shown in Fig. 9, respectively. The close-ups of the red and green rectangles are shown in the right side of each image. As shown in Fig. 9 (b), the aligned FIR image is blurred compared with the visible image, because the original resolution of the FIR image is much lower than the visible one. The result by the existing system show that the artifact is gener-

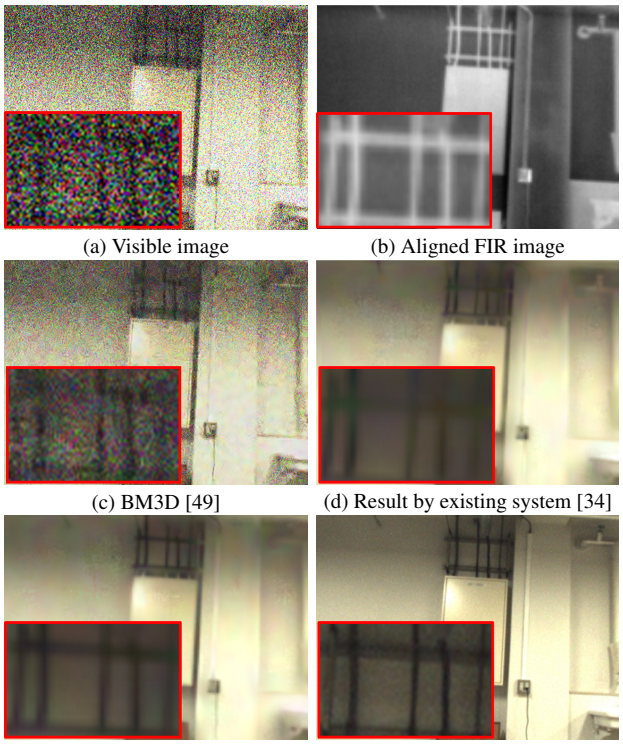

(a) Visible image (b) Aligned FIR image

(c) BM3D [49] (d) Result by existing system [34]

(e) Result by proposed system (f) Ground truth

Figure 8. *Image denosing application.*

ated along the edge of the char as shown in Fig. 9 (c). Furthermore, the structure of the cable fades away by applying the guided filter due to the misalignment. On the other hand, the result by the proposed approach show that the sharp edge of the char and the detail curve of the cable is successfully refined using the visible image as the guide as shown in Fig. 9 (d).

Conclusions

We have presented the novel joint geometric camera calibration framework for the visible and FIR cameras. The main contribution of this paper is to present the simple but accurate calibration for visible and FIR cameras by using the proposed calibration target which is capable of obtaining the clear corresponding points of the checker pattern from the visible and the FIR images. Experimental results showed that the proposed system enables us to easily calibrate the visible and the FIR image with high accuracy compared with a existing method. Furthermore, the proposed system can lead to develop various applications including joint image denoising, and joint image up-sampling.

Acknowledgment: A part of this research was funded by ImPACT Program of Council for Science, Technology and Innovation (Cabinet Office, Government of Japan).

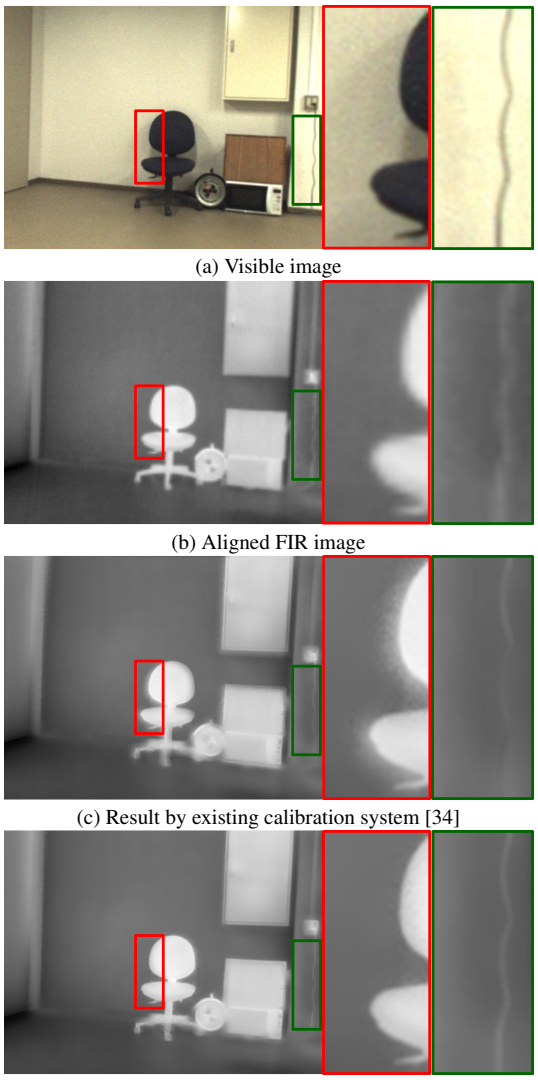

(a) Visible image

(b) Aligned FIR image

(c) Result by existing calibration system [34]

(d) Result by proposed calibration system

Figure 9. *Image up-sampling application.*

References

[1] S. Süsstrunk and C. Fredembach, "Enhancing the visible with the invisible: Exploiting near-infrared to advance computational photography and computer vision," *SID Int. Symposium Digest*, vol. 41, no. 1, pp. 90–93, 2010.

[2] C. Fredembach and S. Süsstrunk, "Colouring the near infrared," *Proc. of the IS&T/SID 16th Color Imaging Conference*, pp. 176–182, 2008.

[3] Lex Schaul, Clément Fredembach, and Sabine Süsstrunk, "Color image dehazing using the near-infrared," *Proc. IEEE Int. Conf. on Image Processing*, , no. LCAV-CONF-2009-026, 2009.

[4] T. Shibata, M. Tanaka, and M. Okutomi, "Versatile visible and near-infrared image fusion based on high visibility area selection," *Journal of Electronic Imaging*, vol. 25, no. 1, pp. 013016–013016, 2016.

[5] G. Piella, "Image fusion for enhanced visualization: A variational approach," *International Journal of Computer Vision*, vol. 83, no. 1, pp. 1–11, 2009.

[6] D. Connah, M. S. Drew, and G. D. Finlayson, "Spectral edge image fusion: Theory and applications," *Proc. of European Conf. on Computer Vision*, pp. 65–80, 2014.

[7] T. Shibata, M. Tanaka, and M. Okutomi, "Multi-spectrum to rgb with direct structure-tensor reconstruction," *Electronic*

Imaging, vol. 2016, no. 18, pp. 1–7, 2016.

[8] A. E. Hayes, G. D. Finlayson, and R. Montagna, "Rgb-nir color image fusion: metric and psychophysical experiments," *IS&T/SPIE Electronic Imaging*, pp. 93960U–93960U, 2015.

[9] G. D. Finlayson and A. E. Hayes, "Iterative spectral edge image fusion," *Proc. of Color and Imaging Conference*, vol. 2015, no. 1, pp. 41–45, 2015.

[10] T. Shibata, M. Tanaka, and M. Okutomi, "Visible and near-infrared image fusion based on visually salient area selection," *Proc. of SPIE Electrical Imaging*, pp. 90230V–1–9, 2015.

[11] Z. Sadeghipoor, Y. M. Lu, and S. Süsstrunk, "Correlation-based joint acquisition and demosaicing of visible and near-infrared images," *Proc. of IEEE Int. Conf. on Image Processing*, pp. 3226–3229, 2011.

[12] D. Krishnan and R. Fergus, "Dark flash photography," *ACM Trans. on Graphics*, vol. 28(3), no. 96, 2009.

[13] E. P. Bennett, J. L. Mason, and L. McMillan, "Multispectral bilateral video fusion," *IEEE Trans. on Image Processing*, vol. 16, no. 5, pp. 1185–1194, 2007.

[14] Y. Monno, S. Kikuchi, M. Tanaka, and M. Okutomi, "A practical one-shot multispectral imaging system using a single image sensor," *IEEE Trans. on Image Processing*, vol. 24, no. 10, pp. 3048–3059, 2015.

[15] N. JW. Morris, S. Avidan, W. Matusik, and H. Pfister, "Statistics of infrared images," *Proc. of the Conf. on Computer Vision and Pattern Recognition*, pp. 1–7, 2007.

[16] M. M. Zhang, J. Choi, K. Daniilidis, M. T. Wolf, and C. Kanan, "Vais: A dataset for recognizing maritime imagery in the visible and infrared spectrums," *In Proc. of IEEE Conf. on Computer Vision and Pattern Recognition Workshops*, 2015.

[17] Matthew Brown and Sabine Süsstrunk, "Multi-spectral sift for scene category recognition," *Proc. of IEEE Conf. on Computer Vision and Pattern Recognition*, pp. 177–184, 2011.

[18] S. Y. Cheng, S. Park, and M. M. Trivedi, "Multiperspective thermal ir and video arrays for 3d body tracking and driver activity analysis," *Proc. of the Conf. on Computer Vision and Pattern Recognition Workshops.*, pp. 3–3, 2005.

[19] F. Xu, X. Liu, and K. Fujimura, "Pedestrian detection and tracking with night vision," *IEEE Trans. on Intelligent Transportation Systems*, vol. 6, no. 1, pp. 63–71, 2005.

[20] O. Tsimhoni, J. Bärgman, and M. J. Flannagan, "Pedestrian detection with near and far infrared night vision enhancement," *LEUKOS*, vol. 4, no. 2, pp. 113–128, 2007.

[21] Y. Fang, K. Yamada, Y. Ninomiya, B. K. P. Horn, and I. Masaki, "A shape-independent method for pedestrian detection with far-infrared images," *IEEE Trans. on Vehicular Technology*, vol. 53, no. 6, pp. 1679–1697, 2004.

[22] M. Bertozzi, A. Broggi, C. Caraffi, M. R. Del, M. Felisa, and G. Vezzoni, "Pedestrian detection by means of far-infrared stereo vision," *Computer Vision and Image Understanding*, vol. 106, no. 2, pp. 194–204, 2007.

[23] N. Yasuda and M. Aoki, "Pedestrian detection and tracking in far infrared images," *Proc. of IEEE Intelligent Transportation Systems*, pp. 182–187, 2005.

[24] R. Du, "Acquisition of 3d surface temperature distribution of a car body," *Proc. of IEEE Information Acquisition*, pp. 5–pp, 2005.

[25] K. Matsumoto, W. Nakagawa, H. Saito, M. Sugimoto, T. Shibata, and S. Yachida, "Ar visualization of thermal 3d model by hand-held cameras," *International Conference on Computer Vision Theory and Applications (VISAPP)*, 2015.

[26] K. Beier and H. Gemperlein, "Simulation of infrared detection range at fog conditions for enhanced vision systems in civil aviation," *Aerospace Science and Technology*, vol. 8, no. 1, pp. 63–71, 2004.

[27] G. D. Finlayson and A. E. Hayes, "Pop image fusion-derivative domain image fusion without reintegration," *In Proc. of IEEE Int. Conf. on Computer Vision*, 2015.

[28] T. Shibata, M. Tanaka, and M. Okutomi, "Unified image fusion based on application-adaptive importance measure," *Proc. of IEEE Int. Conf. on Image Processing*, 2015.

[29] H. Li, B. S. Manjunath, and S. K. Mitra, "Multisensor image fusion using the wavelet transform," *Proc. of IEEE Int. Conf. on Graphical models and image processing*, vol. 57, no. 3, pp. 235–245, 1995.

[30] J. Sun, H. Zhu, Z. Xu, and C. Han, "Poisson image fusion based on markov random field fusion model," *Information Fusion*, vol. 14, no. 3, pp. 241–254, 2013.

[31] S. Li, X. Kang, and J. Hu, "Image fusion with guided filtering," *IEEE Trans. on Image Processing*, vol. 22, no. 7, pp. 2864–2875, 2013.

[32] V. S. Petrovic and C. S. Xydeas, "Gradient-based multiresolution image fusion," *IEEE Trans. on Image Processing*, vol. 13, no. 2, pp. 228–237, 2004.

[33] T. Shibata, M. Tanaka, and M. Okutomi, "Gradient-domain image reconstruction framework with intensity-range and base-structure constraints," *In Proc. of IEEE Conf. on Computer Vision and Pattern Recognition*, 2016.

[34] S. Prakash, P. Y. Lee, T. Caelli, and T. Raupach, "Robust thermal camera calibration and 3d mapping of object surface temperatures," *Defense and Security Symposium*, pp. 62050J–62050J, 2006.

[35] W. Nakagawa, K. Matsumoto, F. D. Sorbier, M. Sugimoto, H. Saito, S. Senda, T. Shibata, and A. Iketani, "Visualization of temperature change using rgb-d camera and thermal camera," *Proc. of European Conf. on Computer Vision Workshops*, pp. 386–400, 2014.

[36] S. Hwang, J. Park, N. Kim, Y. Choi, and I. S. Kweon, "Multispectral pedestrian detection: Benchmark dataset and baseline," *Proc. of IEEE Conf. on Computer Vision and Pattern Recognition*, pp. 1037–1045, 2015.

[37] Z. Zhang, "A flexible new technique for camera calibration," *IEEE Trans. on Pattern Analysis and Machine Intelligence*, vol. 22, no. 11, pp. 1330–1334, 2000.

[38] J. Y. Bouguet, "Camera calibration toolbox for matlab," http://www.vision.caltech.edu/bouguetj/calib_ doc/.

[39] G. Bradski and A. Kaehler, *Learning OpenCV: Computer vision with the OpenCV library*, O'Reilly Media, Inc., 2008.

[40] T. Svoboda, D. Martinec, and T. Pajdla, "A convenient multicamera self-calibration for virtual environments," *PRESENCE: teleoperators and virtual environments*, vol. 14, no. 4, pp. 407–422, 2005.

[41] Z. Yu, S. Lincheng, Z. Dianle, Z. Daibing, and Y. Chengping, "Camera calibration of thermal-infrared stereo vision

system," *Proc. of IEEE Int. Conf. on Intelligent Systems Design and Engineering Applications*, pp. 197–201, 2013.
[42] V. Hilsenstein, "Surface reconstruction of water waves using thermographic stereo imaging," *Image and Vision Computing New Zealand*, pp. 102–107, 2005.
[43] A. Ellmauthaler, E. A. B. Da Silva, C. L. Pagliari, J. N. Gois, and S. R. Neves, "A novel iterative calibration approach for thermal infrared cameras," *Proc. of IEEE Int. Conf. on Image Processing*, pp. 2182–2186, 2013.
[44] M. Gschwandtner, R. Kwitt, A. Uhl, and W. Pree, "Infrared camera calibration for dense depth map construction," *Intelligent Vehicles Symposium (IV)*, pp. 857–862, 2011.
[45] R. Yang, W. Yang, Y. Chen, and X. Wu, "Geometric calibration of ir camera using trinocular vision," *Journal of Lightwave Technology*, vol. 29, no. 24, pp. 3797–3803, 2011.
[46] N. Kim, Y. Choi, S. Hwang, K. Park, J.S. Yoon, and I. S. Kweon, "Geometrical calibration of multispectral calibration," *Proc. of IEEE Ubiquitous Robots and Ambient Intelligence (URAI), 2015 12th International Conference on*, pp. 384–385, 2015.
[47] S. Vidas, R. Lakemond, S. Denman, C. Fookes, S. Sridharan, and T. Wark, "A mask-based approach for the geometric calibration of thermal-infrared cameras," *IEEE Trans. on Instrumentation and Measurement*, vol. 61, no. 6, pp. 1625–1635, 2012.
[48] P. Saponaro, S. Sorensen, S. Rhein, and C. Kambhamettu, "Improving calibration of thermal stereo cameras using heated calibration board," *Proc. of IEEE Int. Conf. on Image Processing*, pp. 4718–4722, 2015.
[49] K. Dabov, A. Foi, V. Katkovnik, and K. Egiazarian, "Color image denoising via sparse 3D collaborative filtering with grouping constraint in luminance-chrominance space," *Proc. of IEEE Int. Conf. on Image Processing*, pp. 313–316, 2007.
[50] K. He, J. Sun, and X. Tang, "Guided image filtering," *Proc. of European Conf. on Computer Vision*, vol. 6311, pp. 1–14, 2010.

Author Biography

Takashi Shibata *received the B.S. and M.S. degrees form the Department of Physics,Tohoku university. in 2005 and 2007, respectively. He joined NEC Corporation in 2008. His research interests include image processing and pattern recognition. He is currently a Ph.D candidate in the Department of Control Engineering, Tokyo Institute of Technology.*

Masayuki Tanaka *received his bachelor's and master's degrees in control engineering and Ph.D. degree from Tokyo Institute of Technology in 1998, 2000, and 2003. He joined Agilent Technology in 2003. He was a Research Scientist at Tokyo Institute of Technology since 2004 to 2008. Since 2008, He has been an Associated Professor at the Graduate School of Science and Engineering, Tokyo Institute of Technology. He was a Visiting Scholar with Department of Psychology, Stanford University, CA, USA.*

Masatoshi Okutomi *received a B.Eng. degree from the Department of Mathematical Engineering and Information Physics, the University of Tokyo, Japan, in 1981 and an M.Eng. degree from the Department of Control Engineering, Tokyo Institute of Technology, Japan, in 1983. He joined Canon Research Center, Canon Inc., Tokyo, Japan, in 1983. From 1987 to 1990, he was a visiting research scientist in the School of Computer Science at Carnegie Mellon University, USA. In 1993, he received a D.Eng. degree for his research on stereo vision from Tokyo Institute of Technology. Since 1994, he has been with Tokyo Institute of Technology, where he is currently a professor in the Department of Mechanical and Control Engineering, the Graduate School of Science and Engineering.*